

Experimental study and calculation of flexural capacity of RC beams strengthened with GFRP sheets

Wang Wenwei¹ Li Guo²

(¹ College of Transportation, Southeast University, Nanjing 210096, China)

(² Department of Civil Engineering, Dalian University of Technology, Dalian 116023, China)

Abstract: Nine reinforced concrete (RC) beams strengthened with glass fiber reinforced polymer (GFRP) sheets and three control beams were tested. Four parameters considered in this experimental program included the concrete strength, the reinforcement ratio, the number of GFRP sheets, and the shear span ratio. It is shown that the application of GFRP sheets can increase the ultimate flexural capacity. The effect of the concrete strength, the reinforcement ratio and the number of GFRP sheets on load capacity is obvious. The shear span ratio can affect the failure mode of RC beams strengthened with GFRP sheets. A theoretical model for flexural behavior of the strengthened RC beam is also developed.

Key words: glass fiber reinforced polymer (GFRP) sheets; strengthen; reinforced concrete (RC) beam; experimental study; flexural capacity

The repair of deteriorated reinforced concrete members using externally bonded fiber reinforced polymer (FRP) laminates has attracted considerable attention in China. FRP systems exhibit several distinct advantages such as lighter weight, higher strength, no corrosion, and easy application procedures at the construction site^[1-3]. Previous laboratory studies have demonstrated effectiveness of externally bonded glass fiber reinforced polymer (GFRP) plates in enhancing both the flexural capacity and shear capacity of concrete beams in China^[4,5]. However, there are a few laboratory researches on GFRP strengthening reinforced concrete (RC) beams. This paper describes the results of experimental and analytical studies concerning the flexural strengthening of reinforced concrete beams by externally bonded GFRP sheets to the **tension face of the beams**.

1 Experimental Program

A total of 12 beams were tested. All beams have

identical rectangular cross-sections and the same size: 150 mm × 250 mm × 2 700 mm (see Fig.1). There are

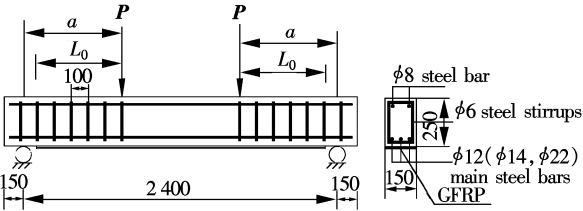


Fig.1 Details of test beams (unit: mm)

three types of shear span length (1 000, 800 and 600 mm) to provide three regions of constant moment: 400, 800 and 1 200 mm. Three beams were used as control specimens and the others were strengthened in flexure using one, two, and three layers of externally bonded GFRP sheets, respectively. Different GFRP lengths with different bond lengths were applied in different beams, respectively (see Tab.1). Three grades of nominal compressive strength of C20, C30 and C40

Tab.1 Test specimens

Beam designation	Grade of concrete strength	GFRP layers	Length of GFRP/mm	Shear span ratio λ	Bond length L_0 /mm	Flexural tension reinforcement ratio ρ_s /%
CL20	C20			4.37		0.70
CL30	C30			3.51		1.43
CL40	C40			2.68		2.36
BL20-1	C20	1	2 300	4.37	950	0.70
BL20-2	C20	2	2 300	3.51	750	1.43
BL20-3	C20	3	2 300	2.68	550	2.36
BL30-1	C30	1	2 100	3.51	650	1.43
BL30-2	C30	2	2 100	3.51	650	1.43
BL30-3	C30	3	2 100	3.51	650	1.43
BL40-1	C40	1	1 900	4.37	750	0.70
BL40-2	C40	2	1 900	3.51	550	1.43
BL40-3	C40	3	1 900	2.68	350	2.36

Received 2003-10-28.

Biography: Wang Wenwei (1971—), male, doctor, lecturer, wenweiw.student@sina.com.

for concrete were used. The flexural tension reinforcement consisted of 12, 14 and 22 mm deformed bars were used. Shear reinforcement consisted of 6 mm round steel stirrups spaced at 100 mm center-center (see Fig. 1). The GFRP material consisted of 150 mm wide and 0.7 mm thick glass sheets that were externally bonded to the tension face of the concrete beams using a two-part epoxy mixed at 2.5 : 1 ratio. The procedures of applying GFRP to concrete involved surface preparation, priming, resin undercoating, glass fiber sheets applying, and resin undercoating. A summary of the material properties is given in Tab.2.

Tab.2 Material properties

Material	f_y /MPa	ε_y /‰	f_u /MPa	ε_u /‰	E /GPa
Steel bar/mm	8	352.1	1.68	523.9	210
	12	381.7	1.91	579.1	200
	14	365.9	1.83	535.9	200
	22	366.5	1.83	541.9	200
Concrete	C20		32.6		30.7
	C30		40.3		32.7
	C40		48.9		34.3
GFRP			542	2.46	22

A total of three linear voltage displacement transducers (LVDTs) were used to measure midspan, and supporting points deflection. All specimens were tested in four points bending over a 2.4 m simple span in a 5 000 kN test frame. All beams were statically tested to failure at a load rate of approximately 12 N/s.

2 Experimental Results and Discussions

Three basic failure modes were exhibited by the

beams strengthened with GFRP sheets, as shown in Fig.2. The load-midspan displacements of experimental beams are shown in Fig.3. The experimental results are summarized in Tab.3.

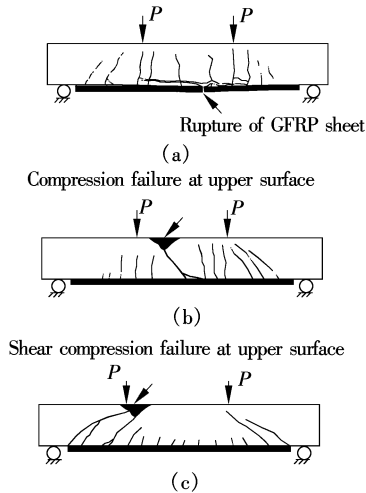


Fig.2 Failure modes

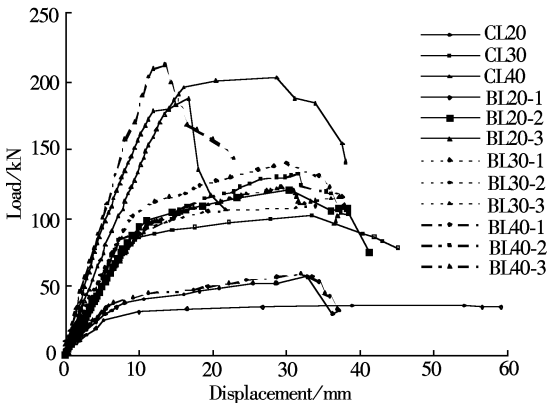


Fig.3 Load-displacement curves for all test beams

Tab.3 Summary of results

Specimen	$P_{\text{yield}}/\text{kN}$	Load at failure				$\Delta_{\text{fail}}/\text{mm}$	Failure mode
		$P_{\text{fail}}/\text{kN}$	Enhancement ratio/%				
			CL20	CL30	CL40		
CL20	30	37				38.9	Crushing of the concrete
CL30	85	102				33.4	Crushing of the concrete
CL40	195	203				28.7	Crushing of the concrete
BL20-1	35	57	54.1			32.8	GFRP rupture
BL20-2	100	120		17.6		30.3	Crushing of the concrete
BL20-3	178	188				16.8	Shear compression
BL30-1	90	110		7.8		33.8	GFRP rupture
BL30-2	100	140		37.3		30.0	Crushing of the concrete
BL30-3	97	123		20.6		29.2	Shear compression
BL40-1	40	60	62.2			31.9	GFRP rupture
BL40-2	85	133		30.4		31.5	Crushing of the concrete
BL40-3	160	213			4.9	13.4	Shear compression

Note: Δ_{fail} is the displacement at failure; P_{yield} is the load at steels yielding.

2.1 Effect of GFRP ratio ρ_f and longitudinal steel ratio ρ_s

The GFRP ratio is defined as the ratio of the cross-section area of GFRP A_f to the area of the

member bh . Because the flexural tension reinforcement ratios of the beams BL20-1, BL30-1 and BL40-1 are relatively low, GFRP force is developed at the ultimate state, resulting in a large increase in the enhancement ratio. The increase ranged between 54.1% and 62.2%

of the load-carrying capacity of the control specimen (beam CL20). As a result of strengthening, there was reduction in beam deflection capacities (see Tab.3).

The two layers of GFRP gave beams BL20-2, BL30-2, and BL40-2, with moderate flexural tension reinforcement ratios, strength gains of 17.6%, 37.3%, and 30.4% over the control beam CL30, respectively. The deflection capacities of beam BL20-2, BL30-2, and BL40-2 were 90.7%, 89.8%, and 94.3%, respectively, of that for control beam CL30.

Three layers of GFRP sheet were externally bonded to the bottom of the beam BL40-3. Furthermore, the beams have more highly longitudinal steel ratios than the other test beams. As a result, 4.9% was the smallest strength increase over the control beam CL40. In the same way, the beams have the lowest deflection capacities. The midspan deflections of beam BL40-3 was 65.9% of that for control beam CL40.

2.2 Effect of GFRP thickness

Fig.4(a) illustrates the relation of GFRP thickness versus the enhancement ratio of ultimate load capacity for beams BL30-1, BL30-2, and BL30-3. It is clear that the ultimate load capacity is enhanced nonlinearly as GFRP thickness increases. Also, it is noted that beam BL30-3, with bonding three layers of GFRP sheets, has changed failure mode from flexural failure to shear compression failure, so its ultimate load capacity is lower than that of beam BL30-2.

Fig.4 (b) shows the ductility index versus GFRP thickness for beams BL30-1, BL30-2, and BL30-3. It is clear that strengthening by externally bonded GFRP

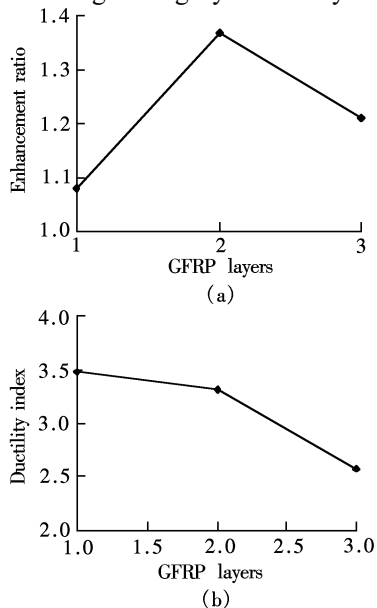


Fig.4 Effect of GFRP layers

sheets can affect the ductility of the strengthened beam. The ductility index, defined as the ratio of the midspan deflection at ultimate load to that at tension steels yielding load, results in significant losses in ductility as GFRP thickness increases.

2.3 Effect of shear span ratio λ

Shear span is defined as the distance a between the support and the nearest concentrated load P action on the top of the beam (see Fig.1). Shear span ratio is the ratio of shear span a to the effective depth of the member h_0 . The effect of shear span ratio on the failure mode of strengthened beams are the same as that of conventional RC beams. The failure mode of strengthened beams gradually changed from the flexural failure mode to the shear compression failure mode with the reduction of the shear span ratio.

2.4 Effect of concrete strength

Fig. 5 shows the relation of concrete strength versus ultimate load capacity for the beams with different GFRP ratios ρ_f . It is clear that concrete strength has a relatively small effect on the ultimate flexural capacity of beams. This effect is relatively pronounced for the beams with higher GFRP ratios.

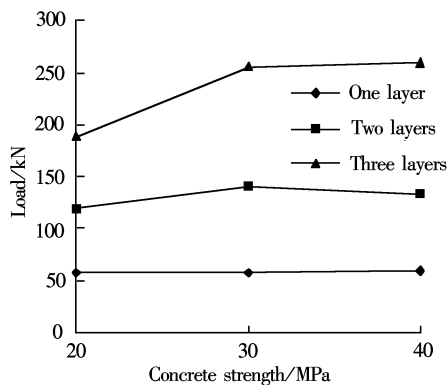


Fig.5 Effect of concrete strength

3 Structural Analysis

There are two types of flexural failure mode according to experimental results. One is the rupture of GFRP; the other is the crushing of the concrete in the compression zone. Some assumptions are made to simplify the problem, which are as follows: ① Plane cross sections remain plane during loadings; ② The stress-strain curve for concrete in compression is the same as that specified in *Code for Design of Concrete Structures* (GB 50010—2002)^[6]; ③ The steel reinforcement bars in both tension and compression are assumed to be elastic before yielding; ④ The stress-strain relationship for GFRP sheet is linear elastic up to rupture; ⑤ The

interface between adhesive and GFRP is considered stronger than the corresponding concrete-adhesive interface. The procedures for analyzing the cross section are presented in the following subsections.

3.1 GFRP rupture

In this case the GFRP attains its ultimate strain before the concrete attains its ultimate strain. Thus, the usual rectangular concrete block assumption at the ultimate state cannot be used. The calculation of the concrete compression force must be performed by integrating the nonlinear concrete stress distribution over the compression area. Such calculations are tedious and complicated, therefore a simple method was proposed using the stress-strain curve for concrete in compression specified in *Code for Design of Concrete Structures*.

The total concrete compression force C_c is given by the following equation:

$$C_c = k_1 f_c b x_0 = \alpha_1 \beta_1 f_c b x_0 = \begin{cases} \left(\frac{\varepsilon_c}{\varepsilon_0} - \frac{\varepsilon_c^2}{3\varepsilon_0^2} \right) f_c b x_0 & 0 < \varepsilon_c \leq \varepsilon_0 \\ \left(1 - \frac{\varepsilon_0}{3\varepsilon_c} \right) f_c b x_0 & \varepsilon_0 < \varepsilon_c \leq \varepsilon_{cu} \end{cases} \quad (1)$$

where b is the width of the cross section, f_c is the concrete cube strength, $k_1 = \alpha_1 \beta_1$, α_1 is the ratio of the average compressive stress to the concrete cube strength, β_1 is the ratio of the depth of the rectangular stress block to the neutral axis depth as shown in Fig.6, x is the depth of the equivalent rectangular concrete stress block, x_0 is the depth of neutral axis, ε_c is the concrete compression strain at the extreme compression fiber, and ε_{cu} is the ultimate compression strain.

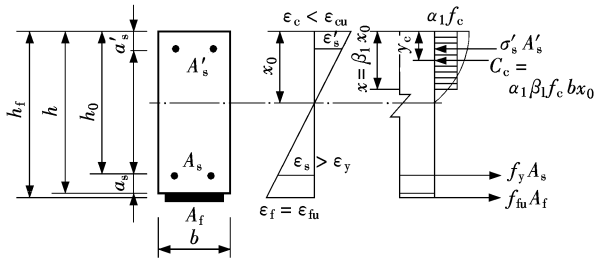


Fig.6 GFRP rupture failure mode

The distance y_c between the centroid of C_c and the extreme compression fiber is determined by

$$y_c = \begin{cases} \frac{4\varepsilon_0 - \varepsilon_c}{12\varepsilon_0 - 4\varepsilon_c} x_0 & 0 < \varepsilon_c \leq \varepsilon_0 \\ 3 - \frac{\varepsilon_0^2}{2\varepsilon_c^2} x_0 & \varepsilon_0 < \varepsilon_c \leq \varepsilon_{cu} \end{cases} \quad (2)$$

$$\frac{\beta_1 x_0}{2} = y_c \quad (3)$$

where

$$\beta_1 = \begin{cases} \frac{4\varepsilon_0 - \varepsilon_c}{6\varepsilon_0 - 2\varepsilon_c} & 0 < \varepsilon_c \leq \varepsilon_0 \\ 2 - \frac{\varepsilon_0^2}{\varepsilon_c^2} & \varepsilon_0 < \varepsilon_c \leq \varepsilon_{cu} \end{cases} \quad (4)$$

$$\alpha_1 = \frac{k_1}{\beta_1} \quad (5)$$

Tab.4 presents the values of α_1 and β_1 for any given concrete compression strain ε_c at the extreme compression fiber.

Tab.4 Values of α_1 and β_1 for any given concrete strain ε_c

ε_c	α_1	β_1	ε_c	α_1	β_1
0.000 5	0.336	0.682	0.002 0	0.889	0.750
0.000 6	0.394	0.685	0.002 1	0.902	0.756
0.000 7	0.449	0.689	0.002 2	0.914	0.763
0.000 8	0.501	0.692	0.002 3	0.923	0.769
0.000 9	0.550	0.696	0.002 4	0.931	0.776
0.001 0	0.595	0.700	0.002 5	0.938	0.782
0.001 1	0.638	0.704	0.002 6	0.944	0.788
0.001 2	0.678	0.708	0.002 7	0.949	0.794
0.001 3	0.714	0.713	0.002 8	0.953	0.799
0.001 4	0.748	0.717	0.002 9	0.957	0.804
0.001 5	0.779	0.722	0.003 0	0.961	0.810
0.001 6	0.807	0.727	0.003 1	0.964	0.814
0.001 7	0.832	0.733	0.003 2	0.967	0.819
0.001 8	0.854	0.738	0.003 3	0.969	0.824
0.001 9	0.873	0.744			

The concrete strain ε_c at the extreme compression fiber is assumed to be less than 0.003 3, and α_1 and β_1 is determined from Tab.4. The neutral axis position is calculated as

$$x_0 = \frac{\varepsilon_c}{\varepsilon_c + \varepsilon_{fu}} h_f \quad (6)$$

where h_f is the depth of GFRP sheet from the top face, ε_{fu} is the ultimate strain of GFRP sheet.

From the equilibrium condition of the forces acting on the cross section, we have

$$\alpha_1 f_c b x_0 + \sigma'_s A'_s = f_y A_s + f_{fu} A_f \quad (7)$$

and

$$\alpha_1 \beta_1 x_0 = \frac{f_y A_s + f_{fu} A_f - \sigma'_s A'_s}{b f_c} \quad (8)$$

where A_s is the area of tension reinforcing steel, A'_s is the area of compression reinforcing steel, A_f is the area of GFRP sheet, f_y is the yield strength of steel.

To determine the neutral axis location, a trial and adjustment procedure is performed by assuming a concrete compression strain ε_c and determining the

corresponding value of α_1 and β_1 in Tab. 4. The neutral axis distance x_0 is then calculated from Eq.(6) and is used to calculate the product $\alpha_1\beta_1x_0$ which is compared to the value obtained from Eq. (8). If the two values for $\alpha_1\beta_1x_0$ are not equal, another value for ε_c is assumed and another iteration is performed. This procedure is continued until two successive values of $\alpha_1\beta_1x_0$ are approximately equal. The moment capacity for the section is then calculated as

$$M = f_y A_s \left(h_0 - \frac{x}{2} \right) + f_{fu} A_f \left(h_f - \frac{x}{2} \right) + \sigma'_s A'_s \left(\frac{x}{2} - a'_s \right) \quad (9)$$

where

$$\sigma'_s = \varepsilon_{fu} E_s \frac{x_0 - a'_s}{h_f - x_0} \quad (10)$$

where a'_s is the effective depth of compression steel, E_s is the modulus of elasticity of steel, f_{fu} is the ultimate strength of GFRP sheet, h_0 is the depth of tension steel from the top face, M is the moment capacity, and σ'_s is the stress of compression reinforcing steel.

3.2 Steel yield-concrete crushing

For section exhibiting this mode of failure, concrete strain at the extreme compression fiber attains the ultimate strain of 0.003 3 and the GFRP strain is less than the ultimate strain as shown in Fig.7. Referring to Fig.7, the cross section equilibrium is established as

$$\alpha_1 f_c b x + \sigma'_s A'_s = A_s f_y + A_f f_f \quad (11)$$

where

$$f_f = E_f \varepsilon_{cu} \left(\frac{\beta_1 h_f}{x} - 1 \right) \leq f_{fu} \quad (12)$$

$$\sigma'_s = E_s \varepsilon_{cu} \left(1 - \frac{\beta_1 a'_s}{x} \right) \leq f_y \quad (13)$$

where $\alpha_1 = 0.969$ and $\beta_1 = 0.824$.

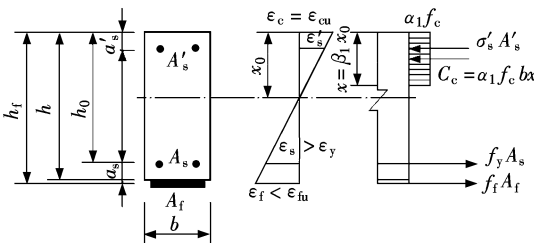


Fig.7 Concrete crushing failure mode

Substituting the expression for GFRP stress f_f given by Eq. (12) and compression steel stress σ'_s given by Eq.(13) into Eq.(11), Eq.(11) can be written as

$$\alpha_1 f_c b x^2 + [(E_s A'_s + E_f A_f) \varepsilon_{cu} - A_s f_y] x - (E_s a'_s A'_s + E_f h_f A_f) \varepsilon_{cu} \beta_1 = 0 \quad (14)$$

Solving Eq. (14) which is quadratic in x , then summing moments about the centroid of the force in the GFRP yields the moment capacity expression:

$$M = \alpha_1 f_c b x \left(h_f - \frac{x}{2} \right) - f_y A_s (h_f - h_0) + \sigma'_s A'_s (h_f - a'_s) \quad (15)$$

To verify the results of the section analysis, a comparison between experimental ultimate loads and calculated ultimate loads is presented in Tab.5. From these results, it is clear that the analytical model is accurate in predicting the ultimate flexural capacity of RC beams strengthened with externally bonded GFRP sheets.

Tab.5 Comparison between experimental and calculated ultimate loads for strengthened beams with GFRP sheets

Beam	Experimental ultimate load/kN	Calculated ultimate load/kN	Difference/%	Mode of failure
BL20-1	57	62.7	10	GFRP rupture
BL20-2	120	132.3	10.3	Concrete crushing
BL30-1	110	115.6	5.1	GFRP rupture
BL30-2	140	130.9	-6.5	Concrete crushing
BL40-1	60	65.2	8.7	GFRP rupture
BL40-2	133	153	15	Concrete crushing
B2 ^[7]	81.25	94.58	16.4	GFRP rupture
6B ^[8]	169.1	157.41	-6.9	Concrete crushing
5B ^[8]	146.85	150.82	2.7	Concrete crushing

4 Conclusions

1) GFRP external reinforcement obviously increased beam ultimate flexural capacities. Beams with lower steel reinforcement ratios exhibited a greater increase in enhancement ratio. This should not be considered a disadvantage since most reinforced concrete structures exhibit relatively low reinforcement ratios.

2) A greater GFRP ratio changed the failure mode from flexural failure to shear compression failure and reduced the ultimate load capacity of the strengthened beams.

3) Shear span ratio mainly affected the failure modes of the test beams. The failure mode of the strengthened beams had gradually changed from flexural failure mode to shear compression failure mode with the reduction of the shear span ratio.

4) Concrete strength has a relatively small effect on the ultimate load capacity of the strengthened beams.

5) A simple approach for analyzing RC concrete beams strengthened with externally bonded GFRP sheets was presented. Excellent correlation of the predicted results with experimental results was noted.

References

[1] Brown V L, Bartholomew C L. FRP reinforcing bars in reinforced concrete members [J]. *ACI Materials Journal*, **1993**, **90**(1): 34 – 39.

[2] Saadatmanesh H, Ehsani M. RC beams strengthened with GFRP plates [J]. *Journal of Structural Engineering*, **1990**, **117**(11): 3417 – 3455.

[3] Saadatmanesh Hamid. Fiber composites for new and existing structures [J]. *ACI Structural Journal*, **1994**, **91**(3): 346 – 354.

[4] Yue Q R, Chen X B, Mu H Y. New technology of carbon reinforced plastics on strengthening & repairing concrete structures [J]. *Industrial Construction*, **1998**, **28**(11): 1 – 5. (in Chinese)

[5] Wu G, Lu Z T. Shear design method of concrete beams strengthened with carbon fiber reinforced polymer sheet [J]. *Industrial Construction*, **2000**, **30**(10): 35 – 38. (in Chinese)

[6] China Concrete Institute. GB 50010—2002 code for design of concrete structures [S]. Beijing: China Construction Industry Press, 2002. (in Chinese)

[7] Arduini M, Tommaso A D, Nanni A. Brittle failure in FRP plate and sheet bonded beams [J]. *ACI Structural Journal*, **1997**, **94**(4): 363 – 370.

[8] Allen R C, Jerome D M, Tedesco J W, et al. Strengthening of reinforced concrete beams with externally bonded composite laminates [J]. *ACI Structural Journal*, **1999**, **96**(2): 212 – 220.

玻璃纤维布加固的钢筋混凝土梁
试验研究与抗弯承载力计算

王文炜¹ 李 果²

(¹ 东南大学交通学院, 南京 210096)
(² 大连理工大学土木系, 大连 116023)

摘要: 对9根玻璃纤维布加固的钢筋混凝土梁和3根对比梁进行了抗弯性能试验研究. 试验中考虑了配筋率、加固量、剪跨比与混凝土强度等级4个参数. 试验结果表明, 经玻璃纤维布加固的钢筋混凝土梁抗弯承载力有显著提高; 混凝土强度、配筋率、加固量对极限荷载有显著影响; 剪跨比对加固梁的破坏形态有影响. 根据不同的破坏模式, 提出了抗弯承载力计算方法.

关键词: 玻璃纤维布; 加固; 钢筋混凝土梁; 试验研究; 抗弯承载力

中图分类号: TU528.043